



## Research article

# Porous carbohydrate–graphene aerogels synthesized by green method as electroactive supercapacitor materials

Hamideh Mohammadian-Sarcheshmeh, Mohammad Mazloun-Ardakani\*

Department of Chemistry, Faculty of Science, Yazd University, Yazd, 89195-741, Iran

## ARTICLE INFO

## Keywords:

Supercapacitor  
Fructose  
Sucrose  
Aerogel

## ABSTRACT

Various graphene derivatives have been known as electrode-active materials for fabricating supercapacitors. Interconnected graphene networks with adjustable porous structures, i.e., 3D graphene aerogels (GAs), can control the restacking of graphene sheets very well and, thus, lead to the enhanced performance supercapacitors. In this study, carbohydrates (sucrose and fructose) were used to make two types of 3D porous carbohydrates–graphene aerogels, sucrose-graphene aerogel (SCR) and fructose-graphene aerogel (FRC). Carbohydrates operate as a cross-linking and reductant agent. Voltammograms of supercapacitor electrodes based on the FRC and SCR indicate a more rectangular shape with a larger area and a superior current than the GA (graphene aerogel without using carbohydrates) electrode. They have better capacitive performance, more electron transportation ability, and higher specific capacitance (CS) values than GA. The supercapacitor electrodes based on FRC, SCR, and GA demonstrate the CS values of  $257.2 \text{ F g}^{-1}$ ,  $221.0 \text{ F g}^{-1}$ , and  $95 \text{ F g}^{-1}$  at  $v = 10 \text{ mV.s}^{-1}$ , respectively. Improvement in the performance of SCR and FRC supercapacitor electrodes, in comparison to GA, is attributed to the porous interconnected feature of their structures and their suitable available surface area, which facilitates electron and ion transportation throughout graphene networks. These supercapacitors also show excellent stability after recording 5000 consecutive voltammograms.

## 1. Introduction

Today, replacing coal and oil with renewable sources such as solar energy, wind energy, and energy storage devices with super efficiency is highly needed [1–4]. Supercapacitors (SCs) have been considered as energy storage devices. Their remarkable power density (P) and excellent stability suggest them for excellent power usage [5,6]. A supercapacitor contains two electrodes with a large surface area (SA) in a liquid electrolyte, including positive (+) and negative (–) ions. A dielectric separator is placed between the electrodes to prevent charge transfer [7]. Some properties have significant effects on the CS value, energy density (E), (P) value, and stability of SCs, for example, the type of electrolytes and their ion size, as well as the electrolyte interaction with the electrodes. The surface features of electrode materials are also crucial for achieving high CS values, expanded potential windows, and, as a result, higher E and P values. Many researchers have shown that surface engineering, optimizing pore sizes, and their distribution and element doping can remarkably enhance the electrochemical performance of electrode materials such as CS, E, and P values and the cycling stability of SCs [8,9].

The most significant electrode active materials for the fabrication of SCs are carbon nanomaterials and different metal compounds

\* Corresponding author.

E-mail address: [mazloun@yazd.ac.ir](mailto:mazloun@yazd.ac.ir) (M. Mazloun-Ardakani).

[10–17]. Carbon nanomaterials with various structural varieties have large SA values. Until now, different carbon materials have been utilized to fabricate SCs, involving carbon nanotubes, active carbons, graphitic carbon, and graphene [18,19]. Among them, graphene and its derivatives are suitable choices for the fabrication of SCs and catalysts [20,21]. Because they have some advantages, such as highly tunable SA, excellent conductivity, and good chemical stability. However, the value of CS obtained from graphene is lower than the expected value due to the aggregation of graphene nanosheets. Thus, modifying the electrochemical performance of graphene-based electrodes is a significant challenge. In this regard, various types of graphene structures have been introduced, including zero-dimensional (0D) (graphene dots), 1D (fibers), 2D (graphene nanocomposites), and 3D (hydrogels and foams). Among these structures, 3D graphene structures with interconnected pores, large SA, and rapid ion/electron transportation are essential for achieving great E and P values and a proper supercapacitance performance [22,23]. GAs, as 3D graphene structures, are ultralight and porous materials with great strength and SA. They also create multidimensional channels to transport ions and electrons and facilitate access to electrolyte solutions [24]. Many researchers have reported applying 3D graphene structures in SCs [25,26]. Many efforts have been made to fabricate SCs through simple and low-cost processes. In this case, producing 3D self-assembled GAs with cross-linked 3D porous structures can be a good strategy [27].

This study is devoted to fabricating GA structures using fructose and sucrose as two kinds of carbohydrates. These structures are applicable as electrode materials in the fabrication of supercapacitors. Sucrose, the ordinary sugar, is classified as a disaccharide. It is composed of two monosaccharides, including glucose and fructose. Fructose, or fruit sugar, is a monosaccharide in many plants and fruits. The fructose structure contains a six-carbon linear chain with hydroxyl and carbonyl groups [28]. Scheme 1. Shows carbohydrate structures.

Some studies were conducted on the structures and electrochemical features of the introduced 3D-GAs to understand the operation of these suggested carbohydrate-based supercapacitors. In this study, a green and environmentally friendly method was used. No toxic, harmful chemicals and organic solvents were used to fabricate the introduced GAs. They were prepared in water solvent using carbohydrates as reducing and cross-linking agents. The manufacturing method did not require very high temperatures. Also, it was cost-effective in terms of manufacturing cost due to the lack of use of chemicals and organic solvents.

## 2. Experiments

### 2.1. Materials

The applied chemicals with analytical grades were purchased from Sigma Aldrich. They are graphite powder, nitric acid, hydrogen peroxide, potassium chloride, fructose, sucrose, sulfuric acid, acetylene black and polytetrafluoroethylene (PTFE), and potassium permanganate.

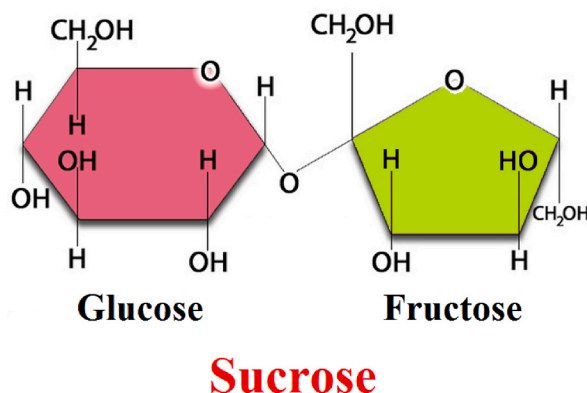
### 2.2. Methods

#### 2.2.1. Characterization

The morphologies were demonstrated by FE-SEM (VEGA\\TESCAN-XMU). X-ray diffraction (XRD) was carried out by a Philips PW1730. FT-IR was examined via a Thermo, AVATAR. The BET measurement was done using BEL, BELSORP MINI II. Raman spectra were recorded by an Almega Thermo Nicolet Dispersive Spectrometer using 532 nm laser light.

#### 2.2.2. Preparation of 3D-graphene aerogels

In the first step, graphene oxide (GO) was fabricated in the same way as the previous articles [29–32] by the following method: (1 g) graphite flakes were added to a mix of  $\text{H}_2\text{SO}_4$  (98 %) and  $\text{H}_3\text{PO}_4$  (85 %) with a volume ratio of 9: 1 and stirred for 3 min. Then, (6 g)  $\text{KMnO}_4$  was added. The solution was stirred at 50 °C for 2 days. Then it was placed in an ice bath. 5 ml of  $\text{H}_2\text{O}_2$  was slowly added to this cold solution to remove any excess  $\text{MnO}_4^-$ . After washing and centrifuging, the product was dried at 80 °C.



Scheme 1. Illustrates fructose and sucrose structures.

In the second step, carbohydrate-based GAs were prepared by a hydrothermal process according to this procedure: (80 mg) GO was added to (40 mL) water and dispersed by ultrasonication for 2 h. Then, 40 ml of the carbohydrate solution ( $4.0 \text{ mg} \cdot \text{mL}^{-1}$ ) was added to the GO solution and dispersed for 1 h. The mixture was treated at  $180^\circ \text{C}$  for 18 h. The product was washed several times and freeze-dried for 24 h to omit water in its structure. The acquired aerogels are introduced as FRC and SCR in this work. GA was fabricated using this method without adding carbohydrates.

### 2.2.3. The preparation of electrode

The work electrodes were made using a slurry. It was prepared with a mixture of 65 wt% of fabricated materials (FRC, SCR, and pure GA), 10 wt% of carbon black, 5.0 wt% of PTFE as a binder, and 20 wt% of graphite powder and ethanol. The slurry was coated on stainless steel grids. The fabricated electrodes were dried at  $80^\circ \text{C}$  for 8 h. Then, electrochemical investigations were done with a three-electrode configuration with the Pt wire (as a counter electrode) and Ag/AgCl (as a reference electrode). Also, 1.0 M KCl served as an aqueous electrolyte. This electrolyte is generally preferred due to its better power output, higher cyclic stability, and inexpensive, environmentally friendly material [33].

Electrochemical investigations involving cyclic voltammetry (CV), galvanostatic charge-discharge (CD), and electrochemical impedance spectroscopy (EIS) were carried out by an Autolab potentiostat/galvanostat (PGSTAT-302 N). The coin-type configuration was utilized as a two-electrode system.

The CS values were calculated for the CV and CD methods through Eq. (1) and Eq. (2), respectively, as follows:

$$CS = \frac{1}{V(V_2 - V_1)} \int_{V_1}^{V_2} I(V) dV \quad (1)$$

$$CS = \frac{I \Delta t}{m \Delta V} \quad (2)$$

The E and the P values were obtained by Eq. (3) and Eq. (4) as follows:

$$E = \frac{CS \cdot \Delta V^2}{7.2} \quad (3)$$

$$P = \frac{3600 E}{\Delta t} \quad (4)$$

where CS ( $\text{F g}^{-1}$ ),  $\Delta V$  (V), m (g), I (A), and  $\Delta t$  (s) are the specific capacitance, potential range, weight of the active materials, current, and discharging time, respectively [34].

## 3. Results and discussion

### 3.1. Characterization

The morphology of FRC, SCR, and GA materials were indicated in Fig. 1(a–c), respectively. It shows the fabricated aerogels have uniform morphologies and suitable interconnected 3D porous networks. The pore sizes of the structures change from sub-micrometers to a few micrometers. It can be observed that the structures of the synthesized materials will change using the two kinds of carbohydrates.

Fig. 2a illustrates the XRD patterns of GA, SCR, and FRC materials. There is no peak at  $10.1^\circ$  for the GA, SCR, and FRC samples, verifying the reduction of GO. In addition, the peaks around  $25^\circ$  and  $43^\circ$ , which are in the (002) and (100) planes for RGO, can verify the reduction of GO during the hydrothermal step [35,36]. The broad peaks for aerogels show a weak ordering of GAs with their stacking direction. Disorders are attributed to intermolecular dehydration and the interaction of different carbohydrates and GAs

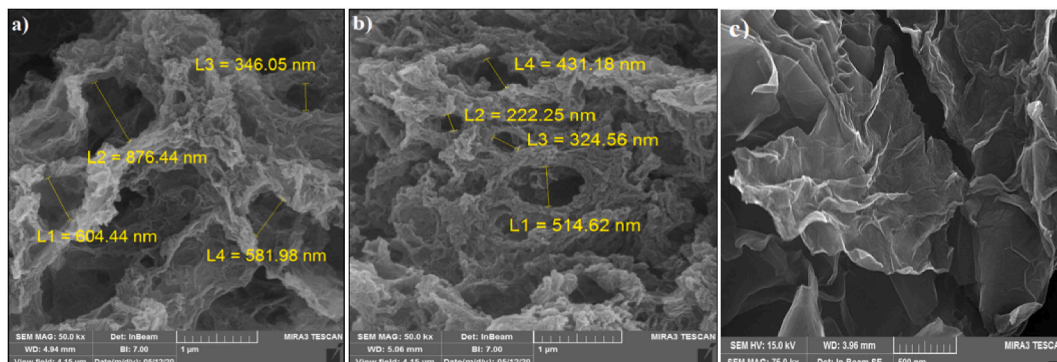


Fig. 1. SEM image results for a) FRC, b) SCR, and c) GA.

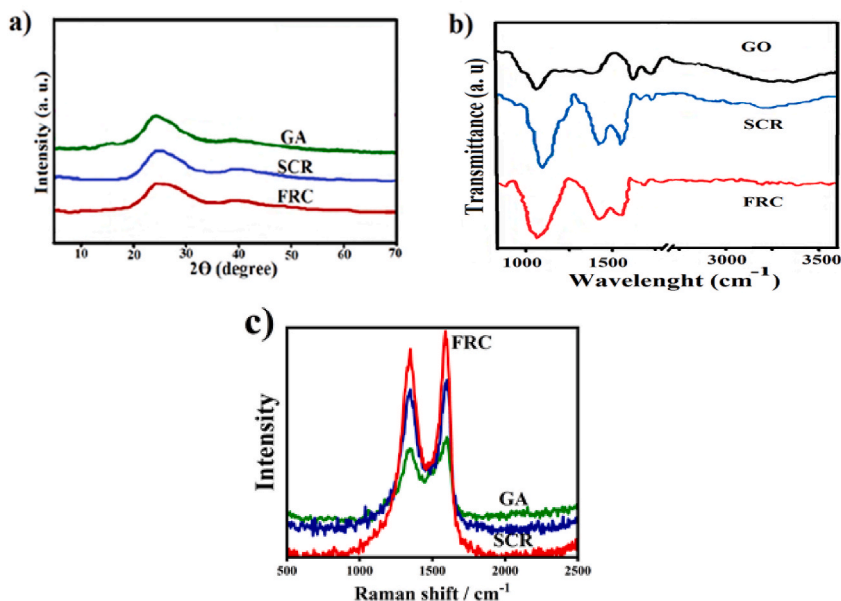


Fig. 2. Comparing of a) XRD results for GA, SCR and FRC, and c) Raman spectra for GA, SCR, and FRC.

throughout the synthesis. Thus, the XRD data indicate that the exfoliation of graphene nanosheets effectively happens in the SCR and FRC materials [37].

The FTIR spectra of GO, FRC, and SCR were compared in Fig. 2b. The spectrum of GO exhibits the presence of an O–H stretching band at 2500–3300  $\text{cm}^{-1}$ , a peak at 1730  $\text{cm}^{-1}$  related to C=O, and a peak at 1110  $\text{cm}^{-1}$  corresponding to the stretching of the C–O band in the C–O–C linkage. FTIR spectra of SCR and FRC show the intensity of the C=O stretching peak and O–H band diminished compared to GO, indicating that GO has been reduced after adding carbohydrates. However, the IR absorption peaks such as C–O stretching, C–O–H bending, and O–H remained due to the presence of carbohydrates. Also, the peaks at 1300–1500  $\text{cm}^{-1}$  correspond to the combination of O–H bending of C–OH indicating the presence of carbohydrates in these structures. Fructose and sucrose do not

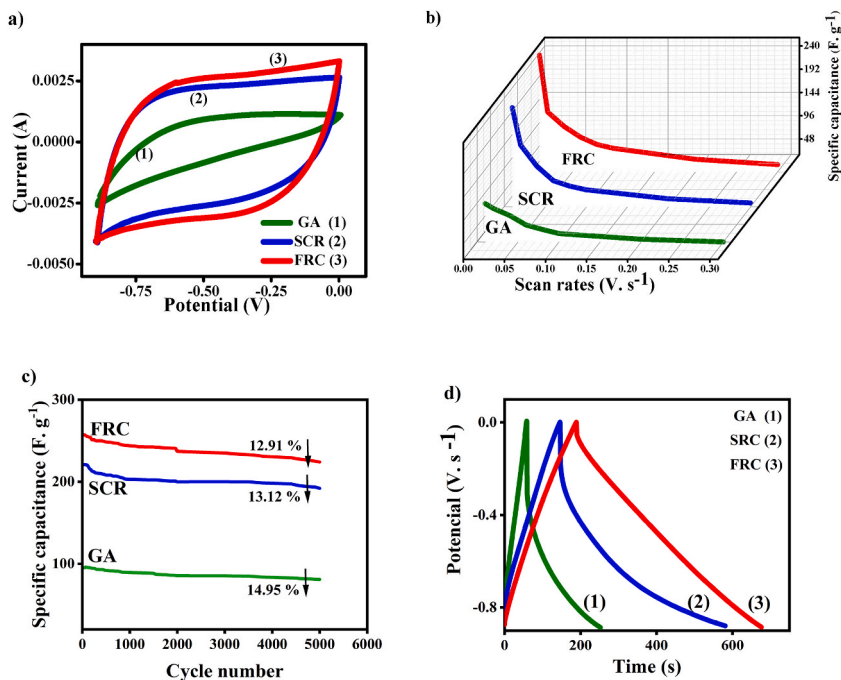


Fig. 3. a) CV voltammograms at  $v = 10 \text{ mV s}^{-1}$ , b) plot of calculated CSs values versus various scan rates, c) comparing of cyclic stability at  $250 \text{ mV s}^{-1}$ , and d) CD curves at  $I = 0.5 \text{ A g}^{-1}$  for FRC, SCR, and GA.

have the C=O group in their structures. The presence of the C=O stretching peak at  $1750\text{--}1735\text{ cm}^{-1}$  can be attributed to the formation of the ester group due to the reaction O–H groups in carbohydrates and C=O in the GO. Appearance of C=O peak at  $1750\text{--}1735\text{ cm}^{-1}$ , increment in the intensity of peak at  $1110\text{ cm}^{-1}$ , and decrease in the intensity of O–H band for the SCR, and FRC confirms the efficient interaction between fructose, sucrose, and graphene nanosheets. According to the results, it is acceptable to say that these GAs were fabricated by co-assembly of carbohydrates and graphene nanosheets. Also, carbohydrates operate as a cross-linking agent [37–42].

In Raman spectra (Fig. 2c), two vibrations of D bands at  $1350\text{ cm}^{-1}$  and G bands at  $1597\text{ cm}^{-1}$  can be seen for GA, SCR, and FRC. The intensity ratios of D and G bands ( $I_D/I_G$ ) were 0.92, 0.94, and 0.97 for GA, SCR, and FRC, respectively. This amount ( $I_D/I_G$ ) for GO is 0.89. The increment in this ratio for synthesized GAs confirms the reduction of GO. It is attributed to removing of oxygen functional groups, which changes the GO structure and introduces some structural defects during the synthesized processes. It shows the improvement of the disordered graphene sheets [43–45].

Fig. S1. Illustrates the Brunauer–Emmett–Teller (BET) results. The SA values for FRC, SCR, and GA are  $104\text{ m}^2\text{ g}^{-1}$ ,  $75\text{ m}^2\text{ g}^{-1}$ , and  $45\text{ m}^2\text{ g}^{-1}$ , respectively. Table S1 Shows total pore volume ( $\text{cm}^3\text{ g}^{-1}$ ) for these samples. These results reveal that carbohydrates have a remarkable effect on creating porous morphologies with better SA value.

### 3.2. Electrochemical measurements

The CV voltammograms of the FRC, SCR, and GA electrodes are compared at the scan rate ( $v$ ) of  $10\text{ mVs}^{-1}$  and a potential range ( $\Delta V$ ) from  $-0.9\text{ V}$  to  $0.0\text{ V}$ . As Fig. 3a indicates, the voltammograms of the FRC and SCR electrode samples have a more rectangular shape, a larger area, and a superior current than that of the GA electrode. They have better capacitive performance, more electron transportation, and higher CS values than GA. The obtained CS values through Eq. (1) are  $257.2\text{ F g}^{-1}$ ,  $221\text{ F g}^{-1}$ , and  $95.0\text{ F g}^{-1}$  for the FRC, SCR, and GA electrodes, respectively. The better supercapacitive functions in the carbohydrate-based electrodes are ascribed to large diffusivity channels, high SA, porosity, and better transportation of electrolytes through their channels. Carbohydrates can serve as spacers to separate graphene nanosheets to create particular morphologies by hydrogen binding reactions between the OH groups in carbohydrates and the oxygen groups in the GO structure. Furthermore, they operate as reductant reagents by omitting the oxygen and COOH groups on GO. Utilization of carbohydrates could improve the conductivity of the fabricated samples [37,46].

Fig. S2. Illustrates the CV plots of the FRC, SCR, and GA samples at various  $v$  values, i.e.  $10.0\text{ mVs}^{-1}$  to  $300\text{ mVs}^{-1}$ , and  $\Delta V = -0.9\text{ V}$ – $0.0\text{ V}$ . The anodic voltammograms moved to larger values at higher  $v$  amount and cathodic potential peaks of voltammograms moved to smaller values at higher  $v$  amount, leading to the polarization phenomenon, and ohmic resistance of the electrodes at large  $v$  values. This means electrochemical behavior is irreversible at larger  $v$  values. The CS values at different  $v$  values were calculated for the FRC, SCR, and GA electrodes. As shown in Fig. 3b, with an increment of  $v$  value, the CS value shows a decreasing trend. The lower CS value at the higher  $v$  amounts is attributed to the decrease of the interactions between electrolyte ions and pores and the occurrence

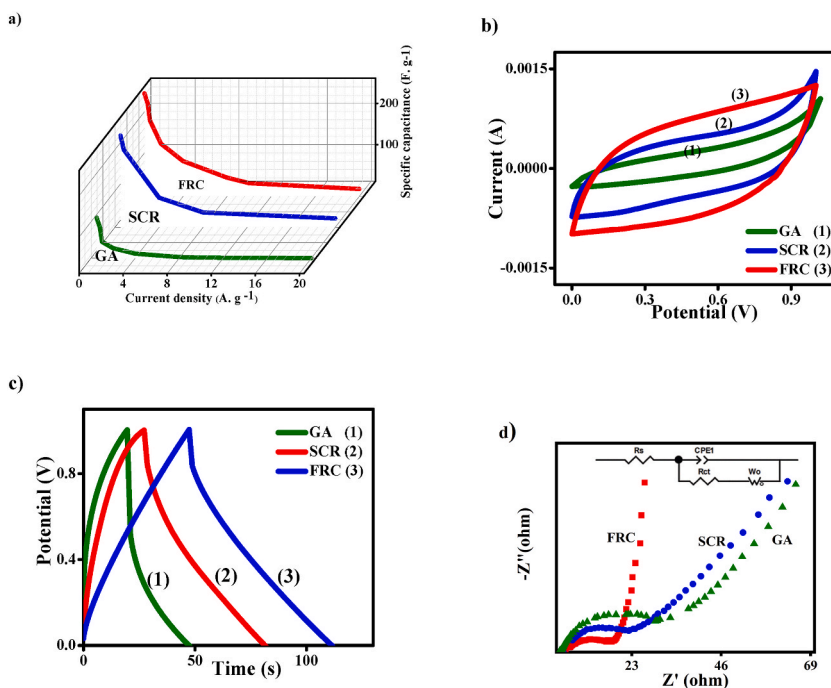


Fig. 4. a) plot of calculated CSs values versus various current density, b) CV voltammograms at  $v = 10\text{ mV s}^{-1}$ , and c) CD curves at  $I = 0.5\text{ A g}^{-1}$ , for a two-electrode system, and d) Nyquist plot for FRC, SCR, and GA electrode materials.

of interactions in the outer area of the electrodes [47].

To comprehend the electrochemical performance of the supercapacitive system, the dependence between the peak current (I) and the  $v$  was examined in CV measurements by Eq. (5):

$$\log I = \log a + b \log v \quad (5)$$

In this equation, (a) and (b) are the constants. The slope of  $\log(I)$  against  $\log(v)$ , (b), is important. If  $b = 1$ , a capacitive process exists. If  $b = 0.5$ , there is a diffusion-controlled process. Also, if  $b$  is 0.5–1, there is a synergistic relation between the diffusion and capacitive processes [48]. The (b) values obtained 0.7, 0.7, and 0.41 for FRC, SCR, and GA, respectively, confirming a better capacitance process for FRC and SCR than GA (Fig. S3).

The cyclic stability, as an important factor in the studies of SCs, was investigated using the CV method by recording 5000 continuous cycles at  $v = 250 \text{ mV} \cdot \text{s}^{-1}$  for all the fabricated electrodes. Fig. 3c displays that the FRC electrode material can keep nearly 87.09 % of its initial CS value, and the SCR and GA electrodes retain 86.88 % and 85.05 % of their initial CS values, respectively.

Fig. 3d compares the CD curves for the FRC, SCR, and GA electrodes at a current density of  $I = 0.5 \text{ A g}^{-1}$  and  $\Delta V = -0.9 \text{ V} - 0.0 \text{ V}$  in a 1.0 M KCl aqueous electrolyte. As can be seen, the FRC and SCR electrodes had a longer discharge time than the GA electrode. Using Eq. (2), the CS values of the electrodes were calculated for the CD curves ( $261.5 \text{ F g}^{-1}$ ,  $234.0 \text{ F g}^{-1}$ , and  $110.0 \text{ F g}^{-1}$  for FRC, SCR, and GA materials, respectively). These CS values confirm the results previously acquired in CV measurements.

Fig. S4 demonstrates the CD curves for different electrodes at various current densities. In addition, Fig. 4a depicts the CS values versus different current densities for the FRC, SCR, and GA active materials. In this study, an increment in the current density resulted in a decrement in the CS value. This is ascribed to the decrease in the discharge time due to the increased carriers and the consequent improvement in the resistance of the electrode samples [49].

A two-electrode system was utilized to examine the electrochemical properties of the introduced supercapacitor. Fig. 4b depicts the CV plots of this system at  $v = 10 \text{ mV} \cdot \text{s}^{-1}$  in the  $\Delta V = 0.0 \text{ V} - 1.0 \text{ V}$ . The calculated CS values were  $62.4 \text{ F g}^{-1}$ ,  $50.0 \text{ F g}^{-1}$  and  $26.7 \text{ F g}^{-1}$  for FRC, SCR and GA, respectively. Fig. 4c indicates the CD curves at  $0.5 \text{ A g}^{-1}$  in  $\Delta V = 0.0 \text{ V} - 1.0 \text{ V}$ . The CS values of this kind of system were calculated according to the reported article [50]. They are  $64.5 \text{ F g}^{-1}$ ,  $55.4 \text{ F g}^{-1}$ , and  $26.6 \text{ F g}^{-1}$  for the FRC, SCR, and GA electrodes, respectively. P and E values are considered the most important factors for comparing energy storage devices. The E value refers to the amount of the stored energy for the unit of mass, but the P value represents the rate of transferred energy in the storage

**Table 1**  
Comparing of suggested materials with other carbohydrate-based electrode materials.

Composite	Electrolyte	Potential area (V)	SC ( $\text{F} \cdot \text{g}^{-1}$ )	Stability	Ref.
FRC	1.0 M	-0.9-0.0	261.5	87.09 %	<b>This work</b>
SCR	KCl		(at $2 \text{ A g}^{-1}$ ) 234.0 (at $0.5 \text{ A g}^{-1}$ )	86.87 % Retention after 5000 cycles	
Glucose GA	1.0 M	-0.2-0.6	161.6	-	[37]
$\beta$ -cyclodextrin GA	1.0 M	-0.2-0.6	130.1	-	[37]
Glucose GA	-	-	145.0	-	[41]
Sucrose GA	-	-	150.3	-	[41]
Graphene based-Chitosan	6.0 M	-1.0-0.0	197	92.1 % after 10000 cycles	[54]
Activated carbon xerogels <sup>a</sup>	1.0 M	-0.2-0.6	153.0	87 % after 10000 cycles	[55]
3D interconnected micro-, meso- and macroporous microsphere <sup>b</sup>	1.0 M	0.0-0.9	164	97 % after 250 cycles	[56]
3D nitrogen-doped GA (NGAs) based on melamine	6.0 M	-0.9-0.0	170.5	82 % after 4000 cycles	[44]
3D sulfur and nitrogen co-doped GA (SNGA)	6.0 M	-1.0-0.0	399	93.3 % after 6000 cycles	[57]
Open-Hollow Nickel-MOFs/Reduced graphene oxide aerogel	6.0 M	0.0-0.5	1644	87.8 % after 10,000 cycles	[58]
3D MXene ( $\text{Ti}_3\text{C}_2\text{T}_x$ ) GA	2.0 M	0.2-1.6	128.6	95 % after 75000 cycles	[59]
	ZnSO4		(at $0.4 \text{ A g}^{-1}$ )		

<sup>a</sup> Fabricated from hydrothermally carbonized glucose- GO hybrids.

<sup>b</sup> Synthesized from aromatic hydrocarbons pyrolysis.

systems [51]. The E ( $\text{Wh kg}^{-1}$ ) and P ( $\text{W kg}^{-1}$ ) were estimated by Eq. (3) and Eq. (4). The maximum E values were 8.96, 7.96, and 3.69  $\text{Wh kg}^{-1}$ . Also, the P values of 517.82, 500.00, and 492.59  $\text{W kg}^{-1}$  were calculated for the FRC, SCR, and GA electrodes, respectively.

The electrochemical performances of the suggested electrodes were further evaluated by electrochemical impedance spectroscopy (EIS) in the frequency area of 0.01 Hz–1 MHz. Fig. 4d compares the Nyquist plots for the SCR, FRC, and GA electrodes. An equivalent circuit model was shown in the inset. ( $R_{ct}$ ) is the charge transfer resistance, ( $R_s$ ) is the solution resistance arising from the electrolyte, CPE is the constant phase element related to the interfacial resistance, and  $Z_w$  is the Warburg impedance. The carbohydrate-based structures indicated a direct line, which largely shifted to an imaginary axis, implying that those structures have an ideal capacitive performance compared to GA electrodes [52]. The  $R_s$  and  $R_{ct}$  values were calculated for all the electrodes. The  $R_s$  amounts were 5.4  $\Omega$ , 6.0  $\Omega$ , and 9.6  $\Omega$ , and the  $R_{ct}$  values were 13.6  $\Omega$ , 17.36  $\Omega$ , and 28.1  $\Omega$  for the SCR, FRC, and GA electrodes, respectively. These results suggest that carbohydrate-based structures have lower resistance and, thus, better ion and charge transfer.

The Bode curves were plotted for electrode materials. The slope of the Bode plots in the low-frequency range was employed to examine the capacitive operation of the samples. A slope value close to 1.0 means ideal capacitive behavior. Fig. S5. Section (a) shows the Bode plot for SCR, FRC, and GA electrodes. The obtained slope values were (−0.64), (−0.60), and 0.42 for the SCR, FRC, and GA electrodes, respectively. The carbohydrate-based supercapacitors showed relatively better capacitive performance than the GA electrode. Fig. S5. Section (b) shows the phase plot for SCR, FRC, and GA electrodes. In the case of phase plots (i.e., the plot of phase versus log frequency), the amount of the phase angle at a small frequency is used to evaluate the capacitance property. The phase angle of (−90°) means an ideal capacitor. The obtained angle values were (−68°), (−53°), and (−40°) for the SCR, FRC, and GA electrodes, respectively. Compared to the GA electrode, the capacitive performance of the carbohydrate-based ones was closer to ideal [53].

Obtained results for this work were compared with the other reported works (Table 1). Our suggested work shows the simplest fabrication method, the highest CS value, and better stability than some of them.

#### 4. Conclusions

Graphene derivatives are attractive electrode materials in the fabrication of supercapacitors. The 1D and 2D forms of these materials have good electrical conductivity and high mechanical flexibility. The performance of the electrodes can be improved if the porous structure providing by reducing the aggregation of graphene nanosheets. This modification leads to the efficient penetration of electrolyte ions, better control of graphene nanosheet restacking, and, thus, enhanced supercapacitor performance. In this study, a green and environmentally friendly method was used. No toxic, harmful chemicals and organic solvents were used to fabricate the introduced GAs. They were prepared in water solvent using carbohydrates as reducing agents. The manufacturing method was not complicated and did not require very high temperatures. Also, it was cost-effective in terms of manufacturing cost due to the lack of use of chemicals and organic solvents. Compared to some similar works presented in Table 1, these materials indicate good capacity and stability. The FRC, SCR, and GA-based supercapacitors provided the CS values of 257.2  $\text{F g}^{-1}$ , 221.0  $\text{F g}^{-1}$ , and 95.0  $\text{F g}^{-1}$ , respectively, at  $v = 10 \text{ mV. s}^{-1}$ . Also, the CS values in the CD technique were 261.5  $\text{F g}^{-1}$ , 234.0  $\text{F g}^{-1}$ , and 110.0  $\text{F g}^{-1}$  for FRC, SCR, and GA materials, respectively, at  $I = 0.5 \text{ A g}^{-1}$ . Carbohydrate structures showed better performance than GA electrode materials. It can be ascribed to the ability of carbohydrates to reduce graphene oxide and produce 3D interconnected GAs with well-expanded porous structures and conductive networks, which can create large ionic pathways for energy storage.

#### Data availability statement

The authors confirm that the data supporting the findings of this study are available within the article and its supplementary materials.

#### CRediT authorship contribution statement

**Hamideh Mohammadian-Sarcheshmeh:** Writing – original draft, Methodology. **Mohammad Mazloum-Ardakani:** Writing – review & editing, Supervision, Conceptualization.

#### Declaration of competing interest

The authors declare that they have no known competing financial interests or personal relationships that could have appeared to influence the work reported in this paper.

#### Acknowledgments

The authors wish to thank the Yazd University Research Council, Iran for financial support of this research.

#### Appendix A. Supplementary data

Supplementary data to this article can be found online at <https://doi.org/10.1016/j.heliyon.2024.e29852>.

## References

- [1] K. Liu, Y. Liu, D. Lin, A. Pei, Y. Cui, Materials for lithium-ion battery safety, *Sci. Adv.* 4 (2018) eaas9820.
- [2] D. Zhou, J. Ni, L. Li, Self-supported multicomponent CPO-27 MOF nanoarrays as high-performance anode for lithium storage, *Nano Energy* 57 (2019) 711–717.
- [3] S. Chu, Y. Cui, N. Liu, The path towards sustainable energy, *Nat. Mater.* 16 (2017) 16–22.
- [4] C.P. Grey, J.M. Tarascon, Sustainability and in situ monitoring in battery development, *Nat. Mater.* 16 (2017) 45–56.
- [5] T. Zhai, S. Sun, X. Liu, C. Liang, G. Wang, H. Xia, Achieving insertion-like capacity at ultrahigh rate via tunable surface pseudocapacitance, *Adv. Mater.* 30 (2018) 1706640.
- [6] Y. Shao, M.F. El-Kady, J. Sun, Y. Li, Q. Zhang, M. Zhu, H. Wang, B. Dunn, R.B. Kaner, Design and mechanisms of asymmetric supercapacitors, *Chem. Rev.* 118 (2018) 9233–9280.
- [7] M.S. Halper, J.C. Ellenbogen, *Supercapacitors: A Brief Overview*, MITRE Nanosystems Group, 2006.
- [8] L. Wan, S. Sun, T. Zhai, S. V Savilov, V. V Lunin, H. Xia, Multiscale porous graphene oxide network with high packing density for asymmetric supercapacitors, *J. Mater. Res.* 33 (2018) 1155–1166.
- [9] W. Yang, W. Yang, L. Kong, A. Song, X. Qin, G. Shao, Phosphorus-doped 3D hierarchical porous carbon for high-performance supercapacitors: a balanced strategy for pore structure and chemical composition, *Carbon* 127 (2018) 557–567.
- [10] J. Rehman, K. Eid, R. Ali, X. Fan, G. Murtaza, M. Faizan, A. Laref, W. Zheng, R.S. Varma, Engineering of transition metal sulfide nanostructures as efficient electrodes for high-performance supercapacitors, *ACS Appl. Energy Mater.* 5 (2022) 6481–6498.
- [11] F. Nemati, M. Rezaie, H. Tabesh, K. Eid, G. Xu, M.R. Ganjali, M. Hosseini, C. Karaman, N. Erk, P.-L. Show, Cerium functionalized graphene nano-structures and their applications; A review, *Environ. Res.* 208 (2022) 112685.
- [12] H. Zuo, W. Fu, R. Fan, D. Dastan, H. Wang, Z. Shi, Bilayer carbon nanowires/nickel cobalt hydroxides nanostructures for high-performance supercapacitors, *Mater. Lett.* 263 (2020) 127217.
- [13] S. Yaglikci, Y. Gokce, E. Yagmur, Z. Aktas, The performance of sulphur doped activated carbon supercapacitors prepared from waste tea, *Environ. Technol.* 41 (2020) 36–48.
- [14] Y. Zhang, H. Chen, S. Wang, X. Zhao, F. Kong, Regulatory pore structure of biomass-based carbon for supercapacitor applications, *Microporous Mesoporous Mater.* 297 (2020) 110032.
- [15] A.M. Teli, S.A. Beknalkar, S.M. Mane, M.A. Yewale, T.D. Dongale, J.C. Shin, Synergetic effect of ternary MnVMO-oxide electrode by hydrothermal method for high-performance asymmetric supercapacitor, *J. Energy Storage* 65 (2023) 107289.
- [16] P.H. Patil, V. V Kulkarni, T.D. Dongale, S.A. Jadhav,  $\alpha$ -Manganese dioxide ( $\alpha$ -MnO<sub>2</sub>) coated with polyaniline (PANI) and reduced graphene oxide (rGO)-Based nanocomposite for supercapacitor application, *J. Compos. Sci.* 7 (2023) 167.
- [17] M.R. Charapale, T.D. Dongale, O.A. Patil, A.M. Teli, S.A. Beknalkar, S.B. Mullani, S.M. Mane, J. Lee, S.A. Masti, Hierarchical 3D flowers of 1T@ 2H-MoS<sub>2</sub> assembled with an array of ultrathin nano-petals for high-performance supercapacitor electrodes, *J. Solid State Electrochem.* 28 (2023) 1–15.
- [18] E.A. Nagelli, L. Huang, A.Q. Dai, F. Du, L. Dai, 3D vertically aligned CNT/graphene hybrids from layer-by-layer transfer for supercapacitors, *Part. Part. Syst. Char.* 34 (2017) 1700131.
- [19] P.H. Patil, S.B. Ravan, S.S. Thoravat, T.D. Dongale, S.A. Jadhav, Synthesis of graphitic carbon from Pisum sativum for supercapacitor applications, *Kor. J. Chem. Eng.* 40 (2023) 2087–2090.
- [20] A.K. Ipadeola, M. Chitt, A. Abdelgawad, K. Eid, A.M. Abdullah, Graphene-based catalysts for carbon monoxide oxidation: experimental and theoretical insights, *Int. J. Hydrogen Energy* 48 (2023) 17434–17467.
- [21] H.I. Abdu, K. Eid, A.M. Abdullah, M.H. Sliem, A. Elzatahry, X. Lu, Dry ice-mediated rational synthesis of edge-carboxylated crumpled graphene nanosheets for selective and prompt hydrolysis of cellulose and eucalyptus lignocellulose under ambient reaction conditions, *Green Chem.* 22 (2020) 5437–5446.
- [22] L. Tang, Y. Wang, Y. Li, H. Feng, J. Lu, J. Li, Preparation, structure, and electrochemical properties of reduced graphene sheet films, *Adv. Funct. Mater.* 19 (2009) 2782–2789.
- [23] H. Chen, M.B. Müller, K.J. Gilmore, G.G. Wallace, D. Li, Mechanically strong, electrically conductive, and biocompatible graphene paper, *Adv. Mater.* 20 (2008) 3557–3561.
- [24] J. Zhang, J. Jiang, X.S. Zhao, Synthesis and capacitive properties of manganese oxide nanosheets dispersed on functionalized graphene sheets, *J. Phys. Chem. C* 115 (2011) 6448–6454.
- [25] L. Wang, X. Ye, P. Zhao, H. Jiang, Y. Zhu, Z. Wan, G. Rao, S. You, G. Zeng, J. Fu, Toward high capacitance and rate capability supercapacitor: three dimensional graphene network fabricated by electric field-assisted assembly method, *Appl. Surf. Sci.* 467 (2019) 949–953.
- [26] M. Ru, A. Huang, J. Hua, R. Huang, S. Yan, Q. Zhang, A novel carbonized natural silk nanofiber/graphene oxide aerogel for supercapacitor, *Mater. Lett.* 359 (2024) 135901.
- [27] Y. Xu, K. Sheng, C. Li, G. Shi, Self-assembled graphene hydrogel via a one-step hydrothermal process, *ACS Nano* 4 (2010) 4324–4330.
- [28] J. Wind, S. Smeeckens, J. Hanson, Sucrose: metabolite and signaling molecule, *Phytochemistry (Elsevier)* 71 (2010) 1610–1614.
- [29] M. Mazloum-Ardakani, F. Sabaghian, H. Naderi, A. Ebadi, H. Mohammadian-Sarcheshmeh, Electrochemical and theoretical study of novel functional porous graphene aerogel-supported Sm<sub>2</sub>O<sub>3</sub> nanoparticles for supercapacitor applications, *J. Solid State Electrochem.* 24 (2020) 1–12.
- [30] M. Mazloum-Ardakani, R. Arazi, Improving the effective photovoltaic performance in dye-sensitized solar cells using an azobenzene-carboxylic acid-based system, *Heliyon* 5 (2019) e01444.
- [31] Z. Souri, M. Mazloum-Ardakani, S. Alizadeh, D. Nematollahi, Template-free electrodeposition of sponge-like porous polymer interwoven with the bi-metallic metal-organic framework and reduced graphene oxide and application in energy storage device, *J. Energy Storage* 55 (2022) 105381.
- [32] F. Jokar, H. Mohammadian, B.B.F. Mirjalili, S.S. Hosseinihah, Electrochemical behavior of benzoxanthene compound in modified glassy carbon electrode by zinc sulfide particles warped in CNT/RGO nanosheets for determination of hydrazine, *Iran. J. Anal. Chem.* 8 (2021) 15–24.
- [33] C. Xu, H. Yang, Y. Li, J. Wang, X. Lu, Surface engineering for advanced aqueous supercapacitors: a review, *Chemelectrochem* 7 (2019) 586–593.
- [34] M. Mazloum-Ardakani, H. Mohammadian-Sarcheshmeh, H. Naderi, F. Farbod, F. Sabaghian, Fabrication of a high-performance hybrid supercapacitor using a modified graphene aerogel/cerium oxide nanoparticle composite, *J. Energy Storage* 26 (2019) 100998.
- [35] H.R. Naderi, M.R. Ganjali, A.S. Dezfuli, P. Norouzi, Sonochemical preparation of a ytterbium oxide/reduced graphene oxide nanocomposite for supercapacitors with enhanced capacitive performance, *RSC Adv.* 6 (2016) 51211–51220.
- [36] A.S. Dezfuli, M.R. Ganjali, P. Norouzi, F. Faribod, Facile sonochemical synthesis and electrochemical investigation of ceria/graphene nanocomposites, *J. Mater. Chem. B* 3 (2015) 2362–2370.
- [37] C.-C. Ji, M.-W. Xu, S.-J. Bao, C.-J. Cai, Z.-J. Lu, H. Chai, F. Yang, H. Wei, Self-assembly of three-dimensional interconnected graphene-based aerogels and its application in supercapacitors, *J. Colloid Interface Sci.* 407 (2013) 416–424.
- [38] M. Ibrahim, M. Alaam, H. El-Haes, A.F. Jalbout, A. de Leon, Analysis of the structure and vibrational spectra of glucose and fructose, *Eclét. Quím.* 31 (2006) 15–21.
- [39] N. V Patil, A.N. Netravali, Multifunctional sucrose acid as a 'green' crosslinker for wrinkle-free cotton fabrics, *Cellulose* 27 (2020) 5407–5420.
- [40] Y.-K. Kim, M.-H. Kim, D.-H. Min, Biocompatible reduced graphene oxide prepared by using dextran as a multifunctional reducing agent, *ChemComm* 47 (2011) 3195–3197.
- [41] J.-L. Zhang, L.-B. Xing, T.-Z. Liu, K. Qin, J. Zhou, H. Cui, S. Zhuo, W. Si, Three-dimensional reduced graphene hydrogels using various carbohydrates for high performance supercapacitors, *J. Nanosci. Nanotechnol.* 17 (2017) 1099–1107.
- [42] C. Zhu, S. Guo, Y. Fang, S. Dong, Reducing sugar: new functional molecules for the green synthesis of graphene nanosheets, *ACS Nano* 4 (2010) 2429–2437.
- [43] L.-B. Xing, J.-L. Zhang, J. Zhang, S.-F. Hou, J. Zhou, W. Si, H. Cui, S. Zhuo, Three dimensional reduced graphene hydrogels with tunable pore sizes using thiourea dioxide for electrode materials in supercapacitors, *Electrochim. Acta* 176 (2015) 1288–1295.

- [44] L.-B. Xing, S.-F. Hou, J. Zhou, J.-L. Zhang, W. Si, Y. Dong, S. Zhuo, Three dimensional nitrogen-doped graphene aerogels functionalized with melamine for multifunctional applications in supercapacitors and adsorption, *J. Solid State Chem.* 230 (2015) 224–232.
- [45] L.-B. Xing, S.-F. Hou, J.-L. Zhang, J. Zhou, Z. Li, W. Si, S. Zhuo, A facile preparation of three dimensional N, S co-doped graphene hydrogels with thiocarbonylhydrazide for electrode materials in supercapacitor, *Mater. Lett.* 147 (2015) 97–100.
- [46] H. Bai, C. Li, X. Wang, G. Shi, A pH-sensitive graphene oxide composite hydrogel, *ChemComm* 46 (2010) 2376–2378.
- [47] A.S. Dezfuli, M.R. Ganjali, H.R. Naderi, P. Norouzi, A high performance supercapacitor based on a ceria/graphene nanocomposite synthesized by a facile sonochemical method, *RSC Adv.* 5 (2015) 46050–46058.
- [48] Y. Song, Z. Chen, Y. Li, Q. Wang, F. Fang, Y.-N. Zhou, L. Hu, D. Sun, Pseudocapacitance-tuned high-rate and long-term cyclability of NiCo<sub>2</sub>S<sub>4</sub> hexagonal nanosheets prepared by vapor transformation for lithium storage, *J. Mater. Chem. A* 5 (2017) 9022–9031.
- [49] X. Lang, H. Mo, X. Hu, H. Tian, Supercapacitor performance of perovskite La<sub>1-x</sub>Sr<sub>x</sub>MnO<sub>3</sub>, *Dalton Trans.* 46 (2017) 13720–13730.
- [50] F. Barzegar, A. Bello, O.O. Fashedemi, J.K. Dangbegnon, D.Y. Momodu, F. Taghizadeh, N. Manyala, Synthesis of 3D porous carbon based on cheap polymers and graphene foam for high-performance electrochemical capacitors, *Electrochim. Acta* 180 (2015) 442–450.
- [51] Z. Ji, X. Shen, H. Zhou, K. Chen, Facile synthesis of reduced graphene oxide/CeO<sub>2</sub> nanocomposites and their application in supercapacitors, *Ceram. Int.* 41 (2015) 8710–8716.
- [52] N. Arjun, G.-T. Pan, T.C.K. Yang, The exploration of Lanthanum based perovskites and their complementary electrolytes for the supercapacitor applications, *Results Phys.* 7 (2017) 920–926.
- [53] M. Shabani-Nooshabadi, F. Zahedi, Electrochemical reduced graphene oxide-polyaniline as effective nanocomposite film for high-performance supercapacitor applications, *Electrochim. Acta* 245 (2017) 575–586.
- [54] P. Hao, Z. Zhao, Y. Leng, J. Tian, Y. Sang, R.I. Boughton, C.P. Wong, H. Liu, B. Yang, Graphene-based nitrogen self-doped hierarchical porous carbon aerogels derived from chitosan for high performance supercapacitors, *Nano Energy* 15 (2015) 9–23.
- [55] M. Enterría, F.J. Martín-Jimeno, F. Suárez-García, J.I. Paredes, M.F.R. Pereira, J.I. Martins, A. Martínez-Alonso, J.M.D. Tascón, J.L. Figueiredo, Effect of nanostructure on the supercapacitor performance of activated carbon xerogels obtained from hydrothermally carbonized glucose-graphene oxide hybrids, *Carbon* 105 (2016) 474–483.
- [56] X. Huang, S. Kim, M.S. Heo, J.E. Kim, H. Suh, I. Kim, Easy synthesis of hierarchical carbon spheres with superior capacitive performance in supercapacitors, *Langmuir* 29 (2013) 12266–12274.
- [57] Q. Liu, L. Zhang, H. Chen, J. Jin, N. Wang, Y. Wang, D. Sui, Sulfur and nitrogen co-doped three-dimensional graphene aerogels for high-performance supercapacitors: a head to head vertical bicyclic molecule both as pillaring agent and dopant, *Appl. Surf. Sci.* 565 (2021) 150453.
- [58] H. Zong, A. Zhang, J. Dong, Y. He, H. Fu, H. Guo, F. Liu, J. Xu, J. Liu, Flexible asymmetric supercapacitor based on Open-Hollow Nickel-MOFs/Reduced graphene oxide aerogel electrodes, *J. Chem. Eng.* 475 (2023) 146088.
- [59] Q. Wang, S. Wang, X. Guo, L. Ruan, N. Wei, Y. Ma, J. Li, M. Wang, W. Li, W. Zeng, MXene-reduced graphene oxide aerogel for aqueous zinc-ion hybrid supercapacitor with ultralong cycle life, *Adv. Electron. Mater.* 5 (2019) 1900537.